UNIVERSITÀ DEGLI STUDI DI BARI

DIPARTIMENTO INTERATENEO DI FISICA

"Michelangelo Merlin"

Livio Nicola Carenza

III Year Report

In this brief essay I will report on the research activity that I carried out during the three years of my PhD.

My research is basically focused on Soft Matter, concerning both Liquid Crystals and Active Matter, from a theoretical perspective. In recent years, many promising applications have boosted increasing interest in these topics which are broadly believed to be key to the design of novel materials with smart properties which may revolutionize the world of visualization devices and medical investigation.

The theoretical description of (living) liquid crystals requires the treatment of the flow $\boldsymbol{v}$ of the underlying fluid and a field theory to capture the physical properties and the dynamics of the suspended units. Hydrodynamics is ruled by a generalized Navier-Stokes equation

$$\rho \left(\partial_t + \boldsymbol{v} \cdot \nabla\right) \boldsymbol{v} = \nabla \cdot \boldsymbol{\sigma}, \tag{1}$$

where the stress tensor $\boldsymbol{\sigma}$ provides a description of the forces which locally act on the fluid elements, ranging from the Newtonian dissipative viscosity to reactive contributions due to the complex inner structure of the fluid. The dynamics of the suspended elements is in turn described by a suitable order parameter ($\boldsymbol{P}$ in the following), evolving in accordance to a advective-relaxing equation:

$$\frac{d\boldsymbol{P}}{dt} = -\Gamma \boldsymbol{h}, \tag{2}$$

where $\boldsymbol{h}$ is a generalized force which drives the system towards its ground state. The coupling of these two equations provides a description of the *nemato-hydrodynamics* –a fascinating field, only partially explored.

In what follows I will first go through a brief introduction concerning the state of the art of theoretical research in Active Fluids and open problems in this scope and I will present a field theory approach for the modelling of (active) liquid crystals and the basic features of the lattice Boltzmann method, the numerical scheme that I implemented to integrate the nemato-hydrodynamic equations. In the following Sections I will present some advancements that I obtained in my research, briefly listed in the following:

- The effect of mirror symmetry breaking at the base of the onset of autonomous motion of droplets of active constituents.
- The development of a novel model to describe confined active gels and smectic liquid crystals and their rheological properties, including negative-viscosity states and superfluidic regime, observed in experiments.
- The Fourier characterization of multi-scale chaotic flows occurring in active gels, resembling those observed in fully developed Kolmogorov turbulence in Newtonian fluids.

1 Theoretical Aspects in Active Matter

Active fluids and gels are living matter or biologically inspired systems composed by self-propelled (or active) units able to convert internal energy into work, giving rise, eventually, to systematic and collective movements. These systems evolve inherently far from thermodynamic equilibrium due to the internal energy injection at a characteristic lengthscale much smaller than the system size.

Living matter offers a wide variety of realizations, ranging from macroscopic scales (flock of birds, schools of fish, insects swarms) to microscopical ones (bacterial suspensions, cytoskeleton extracts). Regardless of the particular realization, active systems often exhibit orientational

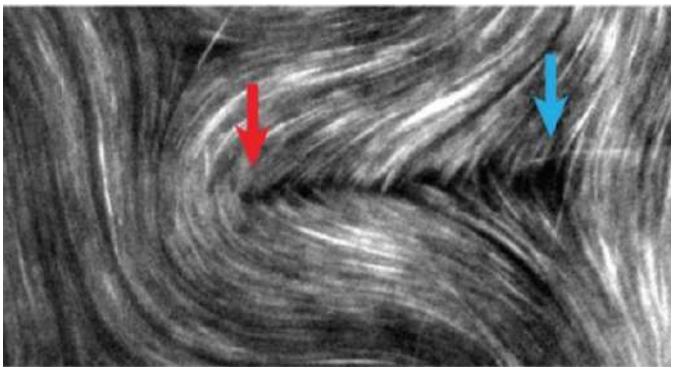

Figure 1: Active microtubule bundles arrange in a nematic fashion. Activity produces flows that advect the constituents eventually leading to the generation of topological defects (see arrows).

order, since fundamental constituents are generally anisotropic, and this defines a preferential orientation for their self-propulsion or the force they apply on their surrounding environment. Anisotropy also leads to effective aligning interactions which lead these systems to exhibit important analogies with passive Liquid Crystals.

At the same time, active systems are characterized by non-equilibrium properties that do not have a *passive* counterpart. One of the key differences is the injection of energy at small scales (i.e. the size of the active agents). This leads to developing hydrodynamic instabilities with a number of fascinating phenomena.

On the experimental side, the complex features of active matter have been widely studied to understand their topological properties, as in the experiment by Sanchez et al.[1], where microtubule filaments were made 'active' by the addition of kinesin, molecular motors capable of converting chemical energy from ATP hydrolysis into mechanical motion of the filaments themselves; at high concentration of the active agents, hydrodynamic instabilities were found to sustain autonomous flows, eventually breaking the long-range orientational order by generating pairs of oppositely charged topological defects (see for instance Fig. 1).

If the strength of active forcing is very intense compared with the elastic properties of the active gel, the dynamics of the system becomes chaotic, a behavior addressed as *active turbulence*. This is highly surprising since biological systems usually evolve at very low Reynolds numbers, due to the reduced length-scale of the flows. Under this conditions, dissipation phenomena overcome advective mechanisms, that are in turn responsible for the onset of classic turbulence in a Newtonian (passive) fluid.

Another fascinating topic in active matter concerns the rheological properties of active fluids. Recently, some experiments have shown the occurence of negative viscosity states in bacterial suspensions. Bacteria are indeed capable of swimming in an ordered fashion, thus exciting flows whose intensity may be orders of magnitude greater than the speed accessible by a single unit. When subject to an external shear, bacteria may organize to counterbalance the imposed flow, by applying a net force on the walls, leading to a situation where the overall behavior of the suspension is similar to a superfluid, eventually inverting the flow, with consequent development of an effective negative viscosity.

Finally, a very relevant point for the control of the dynamics of active systems concerns the case of soft confinement, where active material is emulsified in droplets. Recently, much effort has

[1]Tim Sanchez, Daniel T. N. Chen, Stephen J. DeCamp, Michael Heymann, and Zvonimir Dogic. Spontaneous motion in hierarchically assembled active matter. Nature, 491:431,434, 2012.

been spent to understand if and how confinement can be used to trigger coherent and extended motile states.

2 The lattice Boltzmann Method

Before getting involved in the presentation of the results obtained during my PhD, I will focus in this Section on the lattice Boltzmann method –the numerical approach used to integrate the nemato-hydrodynamic equations.

The lattice Boltzmann approach to hydrodynamics is based on a phase-space discretized form of the Boltzmann equation for the distribution function $f(\vec{r}, \vec{\xi}, t)$, describing the fraction of fluid mass at position $\vec{r}$ moving with velocity $\vec{\xi}$ at time t. Since discretization is performed both in real and velocity space, the algorithm is expressed in terms of a set of discretized distribution functions $\{f_i(\vec{r}_\alpha, t)\}$, defined on each lattice site $\vec{r}_\alpha$ and related to a discrete set of N lattice speeds $\{\vec{\xi}_i\}$, labelled with an index i that varies from 1 to N. In the case of the *collide and stream* version of the algorithm, the evolution equation for the distribution functions has the form

$$f_i(\vec{r} + \vec{\xi}_i \Delta t, t + \Delta t) - f_i(\vec{r}, t) = \mathcal{C}(\{f_i\}, t), \tag{3}$$

where $\mathcal{C}(\{f_i\}, t)$ is the collisional operator that drives the system towards equilibrium, represented by a set of equilibrium distribution functions. Assuming the BGK approximation with a single relaxation time, one writes

$$\mathcal{C}(\{f_i\}, t) = -\frac{1}{\tau}(f_i - f_i^{eq}), \tag{4}$$

where f_i^{eq} are the equilibrium distribution functions and τ is the relaxation time, connected to the viscosity of the fluid. The mass and momentum density are defined as

$$\rho(\vec{r}, t) = \sum_i f_i(\vec{r}, t), \tag{5}$$

$$\rho(\vec{r}, t)\vec{v}(\vec{r}, t) = \sum_i f_i(\vec{r}, t)\vec{\xi}_i, \tag{6}$$

where summations are performed over all discretized directions at each lattice point. By assuming both mass and momentum density to be conserved in each collision, it is found that conditions in Eq. (5), (6) must hold also for the equilibrium distribution functions:

$$\rho(\vec{r}, t) = \sum_i f_i^{eq}(\vec{r}, t), \tag{7}$$

$$\rho(\vec{r}, t)\vec{v}(\vec{r}, t) = \sum_i f_i^{eq}(\vec{r}, t)\vec{\xi}_i. \tag{8}$$

Moreover, it is necessary to introduce further constraints on the second moment of the equilibrium distribution functions to recover continuum equations:

$$\sum_i f_i^{eq} \xi_{i\alpha} \xi_{i\beta} = -\sigma_{\alpha\beta} + \rho v_\alpha v_\beta. \tag{9}$$

Importantly, fluid-dynamics simulation suffer of some computational issue which are long simulation times and large memory allocation. These were addressed through high performance computing techniques, by parallelizing the code via MPI. Further details of the numerical implementations can be found in [5].

3 Rotation and propulsion in 3d active chiral droplets

Many theoretical models have been developed to reproduce the behavior of active sytems in fluid environments, ranging from a molecular dynamic approach (where the dynamics of the single constituents is taken into account) to minimal hydrodynamic approach (as the Slomka-Dunkel model, where super-viscous terms are included to provide energy-injection at small length-scales). In my research I make use of the active-gel model. This is a meso-scale approach where the single constituents are traced out by a coarse-grain over the small length-scales and relevant information is encoded in a few dynamical fields evolving in accordance to suitable evolution equations.

In my research I have made use of this approach to understand the outcome of the interplay between chirality and activity. In stark contrast with the case of achiral active nematics, which has commanded a lot of attention in recent years, very little is known about the dynamics of chiral active systems. I will consider here a system which is *inherently* chiral and apolar, and so can be modelled –in the passive phase– as a cholesteric liquid crystal (CLC). Specifically in [8], we studied a $3d$ active CLC droplet with tangential orientation of the director at its surface. In this setup, an active nematic droplet can only sustain uniform rotational motion, driven by bend deformations localized around the equatorial circle of the droplet. Instead, an intrinsically chiral droplet displays a much richer dynamical behavior. First, we found that a force dipole activity enables a new motility mode, where the rotational motion of the surface defects is converted into propulsion. This mechanism requires chirality to reconfigure the pattern of surface defects. Second, a torque dipole activity sets up a sustained mirror rotation of two pairs of disclinations which periodically adsorb onto and depin from the droplet surface. Again, no such state can be found in an originally nematic system.

3.1 Model

We considered an incompressible fluid with mass density ρ and divergence-free velocity $\mathbf{v}(\mathbf{r},t)$. To characterize the state of the system we introduced two order parameters: a scalar conserved concentration field $\phi(\mathbf{r},t)$ and the $\mathbf{Q}$-tensor that respectively account for the concentration of active material and its orientational order. The equilibrium properties of the system are described by the following Landau-De Gennes free energy functional:

$$\begin{aligned}\mathcal{F}\left[\phi, Q_{\alpha\beta}\right] = \int dV \; \Bigg[& \frac{a}{4}\phi^2(\phi-\phi_0)^2 + \frac{k_\phi}{2}(\nabla\phi)^2 \\ & + A_0\left[\frac{1}{2}\left(1-\frac{\chi(\phi)}{3}\right)\mathbf{Q}^2 - \frac{\chi(\phi)}{3}\mathbf{Q}^3 + \frac{\chi(\phi)}{4}\mathbf{Q}^4\right] \\ & + \frac{K}{2}\left[(\nabla\cdot\mathbf{Q})^2 + (\nabla\times\mathbf{Q} + 2q_0\mathbf{Q})^2\right] + W(\nabla\phi)\cdot\mathbf{Q}\cdot(\nabla\phi)\Bigg] \end{aligned} \tag{10}$$

where the constants a,k_ϕ define the surface tension and the interface width among the two phases, whose minima are found in 0 and ϕ_0. The liquid crystal phase is confined in those regions where $\chi(\phi) = \chi_0 + \chi_s\phi > 2.7$, with $\chi_0 = 10\chi_s = 2.5$. The gradient terms in K_Q account for the energy cost of elastic deformations in the one-constant approximation, while $|q_0| = 2\pi/p_0$, where p_0 is the pitch of the cholesteric helix. Right-handed chirality is achieved by requiring q_0 to be positive. Tangential anchoring is obtained for $W < 0$. The dynamical equations governing the evolution of the system are: (i) a convection-diffusion equation for ϕ

$$\partial_t + \nabla\cdot(\phi\mathbf{v}) = \nabla\cdot\left(M\nabla\frac{\delta\mathcal{F}}{\delta\phi}\right), \tag{11}$$

where M is the mobility parameter; (ii) the Beris-Edwards equation for the $\mathbf{Q}$-tensor:

$$(\partial_t + \mathbf{v}\cdot\nabla)\mathbf{Q} - \mathbf{S}(\mathbf{W},\mathbf{Q}) = \Gamma\mathbf{H}, \tag{12}$$

where we introduced $\mathbf{W} = \nabla\mathbf{v}$ and the strain-rotational derivative

$$\mathbf{S}(\mathbf{W},\mathbf{Q}) = (\xi\mathbf{D}+\mathbf{\Omega})(\mathbf{Q}+\mathbf{I}/3) + (\mathbf{Q}+\mathbf{I}/3)(\xi\mathbf{D}-\mathbf{\Omega}) - 2\xi(\mathbf{Q}+\mathbf{I}/3)Tr(\mathbf{QW}), \tag{13}$$

with $\mathbf{D}$ and $\mathbf{\Omega}$ respectively denoting the symmetric and asymmetric part of $\mathbf{W}$. The parameter ξ controls the aspect-ratio of the liquid crystal molecules and aligning properties to the flow (we chose $\xi = 0.7$ to consider flow-aligning rod-like molecules). On the right-hand side of equation (12) Γ is the rotational viscosity and

$$\mathbf{H} = -\frac{\delta\mathcal{F}}{\delta\mathbf{Q}} + \frac{\mathbf{I}}{3}Tr\left(\frac{\delta\mathcal{F}}{\delta\mathbf{Q}}\right) \tag{14}$$

is the molecular field driving the system towards equilibrium. (iii) The Navier-Stokes equation rules the hydrodynamics of the system:

$$(\partial_t + \mathbf{v}\cdot\nabla)\mathbf{v} = \nabla\cdot\left[\sigma^{pass} + \sigma^{act}\right]. \tag{15}$$

We split the stress tensor contribution in a passive and an active term. The first one accounts for the dissipative/reactive contributions and can be expressed as the sum of the isotropic pressure $\sigma^{hydro}_{\alpha\beta} = -p\delta_{\alpha\beta}$, with p the hydrodynamic pressure and the viscous stress $\sigma^{visc}_{\alpha\beta} = 2\eta D_{\alpha\beta}$, with η the shear viscosity. The relxation dynamics of the two order parameters affect the hydrodynamics through the following passive terms:

$$\sigma^{bm} = \left(f - \frac{\delta\mathcal{F}}{\delta\phi}\right)\delta_{\alpha\beta} - \frac{\delta\mathcal{F}}{\delta(\partial_\beta\phi)}\partial_\alpha\phi, \tag{16}$$

where f is the free energy density,

$$\begin{aligned}\sigma^{el}_{\alpha\beta} = -\xi H_{\alpha\gamma}\left(Q_{\gamma\beta}+\frac{1}{3}\delta_{\gamma\beta}\right) - \xi\left(Q_{\alpha\gamma}+\frac{1}{3}\delta_{\alpha\gamma}\right)H_{\gamma\beta} \\ + 2\xi\left(Q_{\alpha\beta}-\frac{1}{3}\delta_{\alpha\beta}\right)Q_{\gamma\mu}H_{\gamma\mu} + Q_{\alpha\gamma}H_{\gamma\beta} - H_{\alpha\gamma}Q_{\gamma\beta}.\end{aligned} \tag{17}$$

The active stress tensor is a phenomenological contribution derived from a coarse graining procedure. In general, the propulsive motion of active agents dispersed in a fluid creates a circulating flow pattern around each swimmer. The specific swimming mechanism of bacteria, for example, causes fluid to be expelled both forwards and backwards along the fore-aft axis, and drawn inwards radially towards this axis, creating an extensile flow pattern. In some cytoskeleton extracts (such as the actomyosin protein complex), motor proteins can pull the filaments amongst themselves, causing them to contract lengthwise and giving rise to a contractile flow opposite to that described for extensile stresses (Fig. 2). By summing the contributions from each force dipole and coarse-graining[2], it is possible to show that the stress exerted by the active agents can be expressed as

$$\underline{\underline{\sigma}}^{act} = -\zeta\phi\boldsymbol{Q}$$

where ζ is the active parameter or simply activity that rules the intensity of the stress exerted by the active agents. The sign of ζ allows for distinguishing between extensile ($\zeta > 0$) and contractile ($\zeta < 0$) suspensions.

[2]Y. Hatwalne, S. Ramaswamy, M. Rao, and R.A. Simha. Rheology of active-particle suspensions. Phys. Rev. Lett., 92:118101, 2004.

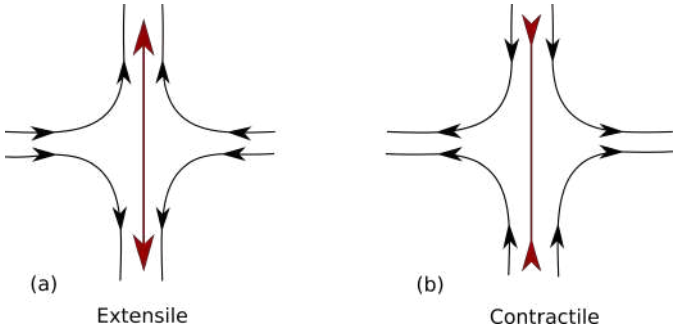

Figure 2: Cartoon of (a) extensile and (b) contractile flow (black lines), and force dipoles (red arrows).

3.2 Cholesteric droplet with active force dipoles: screwlike propulsion

I will now consider the case of a cholesteric droplet, still with active force dipoles only. The two key control parameters are now θ and N. For a fixed value of N, increasing ζ again leads to three possible regimes. For sufficiently large cholesteric power (e.g., $N = 2$, Fig. 3) the surface defect pattern is a pair of nearby $+1$ defects, reminiscent of a *Frank-Price structure* which is seen in passive cholesterics, but only with much larger N ($N \geq 5$). The configuration of director field which we observe is known as *radial spherical structure*, with some additional distortions in the cholesteric layers due to activity (as suggested by the inset in Fig. 3g that gives an insight into the cholesteric arrangement in the interior of the droplet). There is a suggestive analogy between this structure and a magnetic monopole – representing the radial orientation of the helical structure at the droplet centre – with its attached *Dirac string*, joining the centre of the droplet with the defect pair. In our simulations the latter represents the region of maximal layer distortion and energy injection, as suggested by the intensity of the velocity field, plotted in Fig. 3g.

The two surface defects rotate around each other: as they do so, the pair periodically separates and reconvenes. At the same time, the droplet undergoes a global rotation with oscillating angular velocity (Fig. 3h). Remarkably, this time the rotation is accompanied by a translation along the direction of the rotation axis – thereby resulting in a screwlike motion, with the axis of the rototranslation parallel to the *Dirac string*. This motility mode is compatible with the chiral symmetry of the system, which introduces a generic non-zero coupling between rotations and translations. Strong deformations induced by the two close rotating $+1$ defects are responsible of the intense flows that develops internally at the droplet and is maximum at the rear (see Fig. 3g) thus powering propulsion. Symmetry of the flow corresponds to that of a macroscopic pusher. Mechanistically, therefore, activity is required to power droplet rotation, and chirality is needed to couple rotation to motion. As the motion is screwlike, the linear and the angular velocity are proportional to each other – a similar argument to that used for active nematics also shows that they should both scale approximately linearly with θ, and we found this to hold for our simulations (Fig. 3h, inset).

A phase diagram in a portion of the (N, ζ) plane is shown in Fig. 3i. The results show that for small activity the droplet sets into a quiescent regime indipendently of the cholesteric power: this is characterized by weak bending deformation of the LC network on the droplet surface, which are not enough to power any self-sustained motion. As activity is increased different behaviors arise: for null or weak cholesteric power ($N \leqslant 1$) stationary rotational motion sets up while screwlike propulsion needs the defects to relocate to one hemisphere creating a dipolar pattern. This is found to be only possible for a limited range of ζ and only for $N = 2, 3$. Indeed, at higher

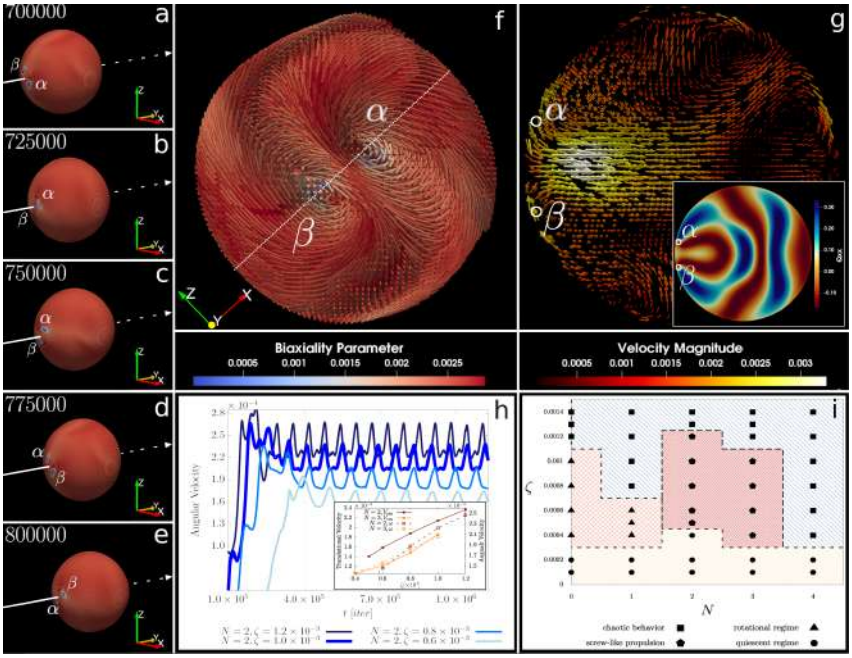

Figure 3: *Screw-like propulsion in a chiral droplet with active force dipoles.* Panels (a-e) show snapshots at different times of a chiral active droplet for the case at $N = 2$ and $\zeta = 10^{-3}$. The contour-plot of the biaxility parameter on the droplet surface serves to identify the position of the two $+1$ defects, labelled with greek characters α and β, whose configuration can be appreciated by looking at panel (f). The screw-like rotational motion generates a strong velocity field in the interior of the droplet in proximity of the two defects. The velocity field has been plotted in panel (g) on a plane transversal to the plane of rotation of the two defects (dashed line in panel (f)). The inset shows the contour plot, on the same plane, of the Q_{xx} component of the Q-tensor, exhibiting an arrangement similar to the *radial spherical structure*. Panel (h) shows the time evolution of the angular velocity of the droplet for some values of ζ. The inset shows the mean angular velocity and the translational velocity of the droplet as a function of ζ both for $N = 2$ and $N = 3$. Panel (i) summarizes the droplet behavior as a function of ζ and N.

cholesteric power ($N \geqslant 4$), the droplet sets into the chaotic phase even at intermediate activity, a regime characterized by defect nucleation and disordered droplet motility that can be found at any N for sufficiently large values of ζ.

4 A continuum model for active emulsions

Recent experiments have shown that is possible to obtain systems with many suspended droplets in a passive matrix, paving the way towards morphological control and dynamical syncronization of the flow state of large stack of active material over scales much larger than a single drop. Active emulsions are indeed a challenging class of systems with many potential novel applications as they may be used as building-blocks for designing novel active soft materials with smart properties.

In order to describe a suspension of active constituents a concentration (scalar) field ϕ is used, while their mean (local) orientation is given by the polarization (vector) field $\boldsymbol{P}$. The velocity field $\boldsymbol{v}$ is assumed to be divergence-free, since in experiments on active fluids comprimibility effects are highly suppressed (*i.e.* the density ρ is uniform and constant) as the velocity are very low ($\sim 10\mu m/s$).

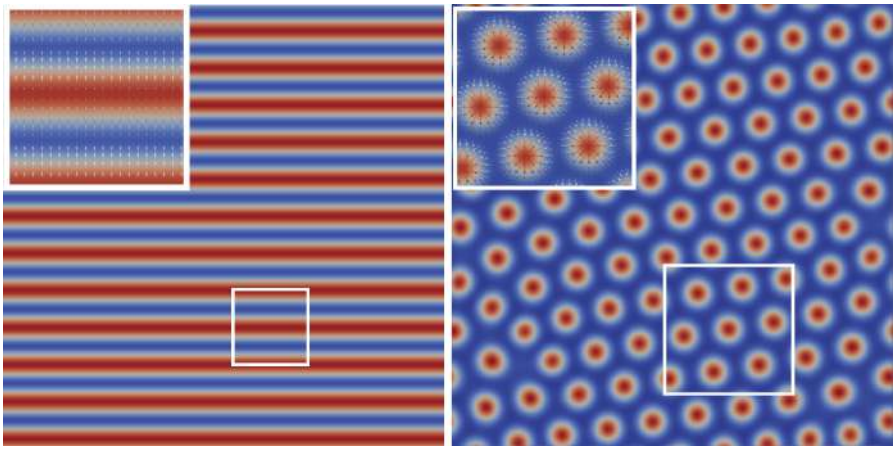

Figure 4: Configuration of a polar binary mixture during the relaxing dynamics for symmetric and asymmetric compositions, respectively shown in the left and right panels.

By assuming that the amount of active constituents is conserved, one can require the dynamics of the concentration ϕ to be ruled by the convection diffusion equation Eq, (11). The polarization field follows a Beris-Edwards evolution:

$$\frac{\partial \boldsymbol{P}}{\partial t} + (\mathbf{v} \cdot \nabla)\, \boldsymbol{P} = -\boldsymbol{\Omega} \cdot \boldsymbol{P} + \xi \boldsymbol{D} \cdot \boldsymbol{P} - \Gamma \boldsymbol{h}. \tag{18}$$

Γ is the rotational viscosity and $\boldsymbol{h} = \delta \mathcal{F}/\delta \boldsymbol{P}$ is the molecular field that drives the fields towards the equilibrium configuration defined by the free energy functional $\mathcal{F}$ which will be defined in the following. The hydrodynamics is governed by the Navier-Stokes equation Eq. (15).

In the follwing I will present some studies on a polar active emulsion, whose equilibrium property is encoded in the following free-energy, a generalization of the Landau-Brazovskii theory, coupled to the De Gennes theory for liquid crystals [1,2]:

$$\begin{aligned} \mathcal{F}\left[\phi, \boldsymbol{P}\right] = \int \mathrm{d}\boldsymbol{r} \Bigg[& \frac{a}{4\phi_{cr}^2}\phi^2(\phi-\phi_0)^2 + \frac{k_\phi}{2}(\nabla\phi)^2 + \frac{c}{4}(\nabla^2\phi)^2 \\ & -\frac{\alpha}{2}\frac{(\phi-\phi_{cr})}{\phi_{cr}}\boldsymbol{P}^2 + \frac{\alpha}{4}\boldsymbol{P}^4 + \frac{k_P}{2}(\nabla \boldsymbol{P})^2 + \beta \boldsymbol{P}\cdot\nabla\phi \Bigg]. \end{aligned} \tag{19}$$

Here the first term is a double well potential for the concentration field allowing for the phase separation of the two fluids when $a > 0$, the gradient term propotional to $k_\phi < 0$ sets the surface tension that is negative in this case to favour the formation of interfaces, while the last term is required for thermodynamic stability. The polarization field $\boldsymbol{P}$ is confined in those regions where $\phi > \phi_{cr}$, while the gradient term for $\boldsymbol{P}$ defines the elastic properties of the polar liquid crystal. The last term anchors the polarization field to the interfaces (anchoring is tangential if $\beta < 0$ or hometropic if $\beta > 0$). The theory has a transition to a lamellar phase for $a < \frac{k_\phi^2}{4c} + \frac{\beta^2}{k_P}$, for symmetric compositions of the mixture [6]. In what follows I set the parameters of the free energy to ensure to be deeply in the lamellar phase. A typical configuration of the passive system during the relaxing dynamics is given in Fig 4 (left panel) [2]. When the composition of the mixture is sufficiently asymmetric, the lamellar pattern becomes unstable and gives way to an emulsion of droplet of the minority component in a matrix of the majority phase [1,3,4].

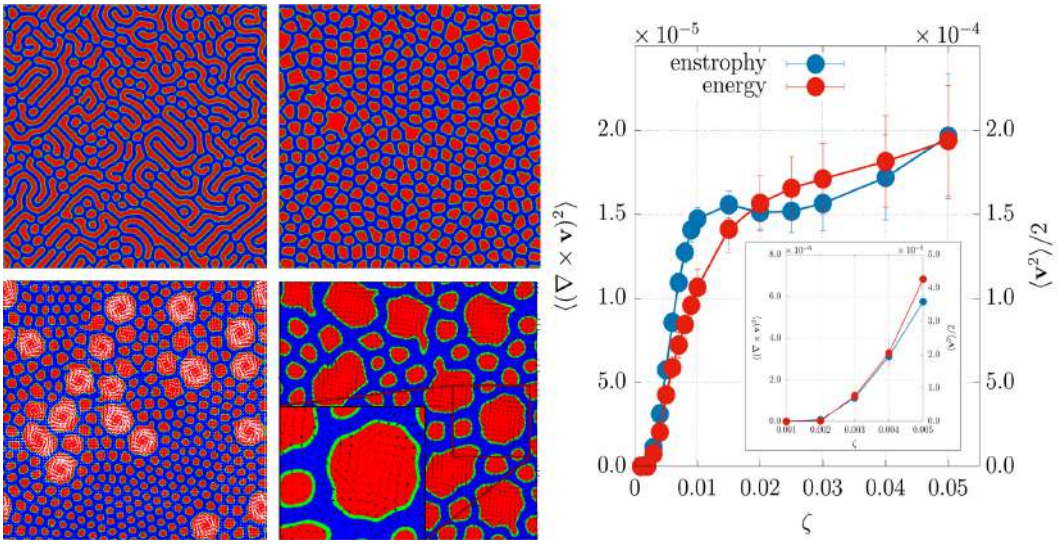

Figure 5: (Left) Late time contour plots of ϕ for $50:50$ extensile mixtures. (Top, left) $\zeta = 0.001$; (top, right) $\zeta = 0.002$; (bottom, left) $\zeta = 0.003$; (bottom right) $\zeta = 0.004$. Extensile activity leads to an emulsion of active droplets within a passive background. For moderate activity larger droplets rotate, as depicted by white velocity vectors in the bottom left panel. The zoom at $\zeta = 0.004$ illustrates typical polarisation patterns (black vectors in bottom the right panel) that have either an aster-like structure in small non-rotating droplets or a spiral shape in big rotating ones. (Right) Plot of the mean kinetic energy and of the mean enstrophy for several values of the extensile activity.

5 Morphology of active emulsions

Experiments and numerical simulations performed on active matter suggest that three dynamical regimes develop in active gels at varying the activity parameter ζ: a quiescent regime where dissipative effects locally dissipate energy injected by activity and no flow is developed, an intermediate regime where elastic and active effects counterbalance and eventually give rise to spontanoeus flow and periodic behaviors, and finally a chaotic regime when activity overcomes reactive effects and push the system towards a turbulent-like state. The transition from the quiescent state first towards the spontaneous motion regime then to active turbulence strongly affects the morphology of active emulsions.

Extensile mixtures In the present Section I consider the case in which the active component is extensile ($\zeta > 0$) [2]. Upon increasing ζ the lamellar phase immediately gives way to an emulsion of active droplets within a passive background (Fig. 5) – the inverse of what happens in contractile mixtures. The active droplet emulsion is approximately monodisperse for $\zeta = 0.002$ (top right panel), and bidisperse for $\zeta = 0.003$ (bottom left panel). The transition between the lamellar and emulsion morphologies corresponds to the value of activity for which the mean enstrophy and kinetic energy depart from zero, $\zeta_{cr} \simeq 0.002$. The droplet size increases monotonically with the activity parameter – again the opposite behaviour of contractile mixtures. At very large ζ there is a crossover to macroscopic phase separation between active and passive components (corresponding to the plateau in the enstrophy and kinetic energy plots in Fig. 5), whereas for higher values of ζ the demixing process stops.

If an asymmetric active emulsion where the active and passive phase are in a ratio of $25:75$ [8]

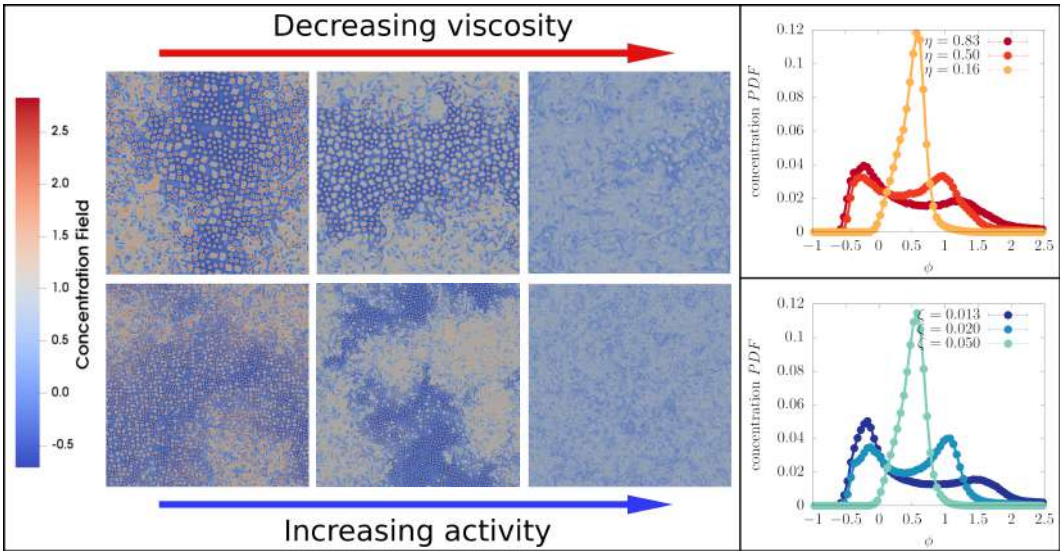

Figure 6: (Top-Bottom) Late time contour plots of ϕ for 25 : 75 extensile mixtures and its *pdf* at varying viscosity-activity.

is considered the equilibrium configuration of the system is not anymore showing lamellar patterns but an emulsion of droplets of the minority component in a majority background that arrange in an hexaticly orered fashion, eventually with some lattice defects in the whole pattern (see for instance the right panel of Fig. 4). As activity is switched on fluxes strengthen throughout the system and, analogously to what happen in the contractile symmetric case, they favor the elimination of topological lattice defects. Eventually, the system ends up in a defect free configuration at low-intermediate values of activity. Nevertheless, when ζ is increased over a certain threshold, droplets of active material may merge giving way to the onset of bending instabilities of the confined polar liquid crystal. This, firstly brings the droplet to rotate in a similar fashion as in the bottom contour plots of Fig. 5 but when activity is further increased the system undergoes a new morphological transition towards a total mixed phase, different from the one previously analyzed. This is due to the fact that strengthening the doping, induces more and more active stress across the droplets leading to interface breaking and droplet coalescence. The consecutive dispersion of active agents in the whole volume has the important effect to change the typical flow length-scales since small-scale deformation of the polarization pattern are wiped out.

Fig. 6 shows that the increase of the activity parameter is basically equivalent to an effective reduction of the viscosity of the mixture. This suggests an analogy between the mechanism driving newtonian fluids towards hydrodynamic turbulence and the chaotic dynamics of active gels, which will be presented in the next Section.

6 Active Turbulence in Extensile Active Gels

Hydrodynamic turbulence is the last open problem in classical physics and no comprehensive theory has ever been formulated so far. The main problem concerning turbulence is the onset of hydrodynamic instabilities driven by the non-linear advection term $(\boldsymbol{v} \cdot \nabla \boldsymbol{v})$ in the Navier-Stokes equation. For a newtonian fluid there exists a single control parameter that is the Reynolds

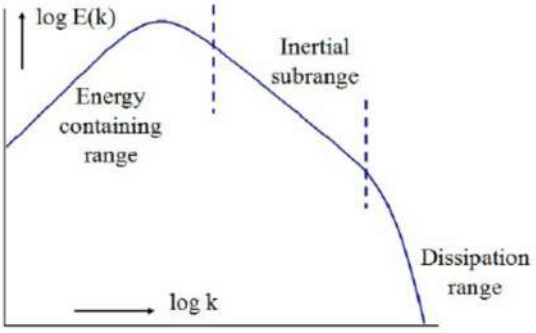

Figure 7: Typical energy spectrum of a turbulent flow in a newtonian fluid.

number

$$Re = \frac{l^* v^*}{\eta},$$

where l^* and v^* are respectively the typical length and speed of the flow, while η is the shear viscosity appearing in the viscous stress tensor. When the Reynolds number is low (hence when the velocity is very low or the flow length-scales are small so that dissipation phenomena overcome momentum advection) the fluid is in the laminar regime and flows in an ordered fashion; but when $Re \gtrsim 2700$ the transition to turbulence occurs, since energy is advected through different length-scales until it is dissipated at the micro-scales by viscous (molecular) phenomena.

To better understand the partition of energy between different length-scales it is custom in fluid-dynamics to study the statistical properties of the flow by looking at the energy spectrum, namely the spherical averaged structure factor of the flow field:

$$E(k) = \langle \boldsymbol{v}(\boldsymbol{k})^* \cdot \boldsymbol{v}(\boldsymbol{k}) \rangle,$$

where $\boldsymbol{v}(\boldsymbol{k})$ is the Fourier transform of the velocity field, and $\langle \cdot \rangle$ denotes spherical average. The typical shape of the energy spectrum is shown in Fig. 7. Three different regions can be found: at large length-scales (hence at low wave-numbers) the spectrum increases towards the peak where energy is accumulated and for this reason is usually addressed as *energy containing range*. This lenght-scale usually corresponds to the typical scale where energy is pumped into the system. In the *inertial range* energy is transferred by means of advective phenomena towards smaller scales, where viscosity will dissipate energy by means of friction mechanisms (the range of scales where viscosity becomes important is then addressed as *dissipation range*). According to Kolomogorov's theory, the flow must be self-similar in the inertial range where the only effective mechanism is the energy transfer due to the advective non linearity. By simple dimensional arguments, Kolmogorov proved that the energy spectrum in this range must satisfy the power low

$$E(k) \sim k^{-5/3},$$

a trand that is the universal fingerprint of fully developed hydrodynamic turbulence and it is found in any turbulent newtonian fluid.

In what follows I will present the results of my study on active turbulence that I performed by applying typical hydrodynamic methods to an unconfined active gel.

Our approach to quantitatively study the response of elastic and dissipative contributions to active injection is to consider a balance equation for the kinetic energy in Fourier spacen:

$$\partial_t E_k + \mathcal{T}_k = \mathcal{S}_k^{visc} + \mathcal{S}_k^{el} + \mathcal{S}_k^{act}, \tag{20}$$

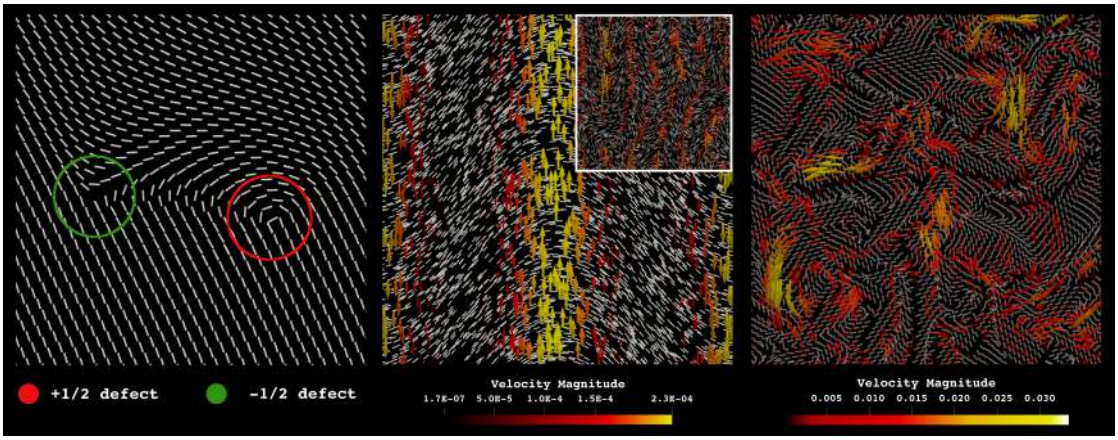

Figure 8: **Dynamical regimes of active nematics.** Numerical simulations of an active nematics with elastic constant $K = 0.04$ at varying the intensity of the activity ζ. The picture is a summary of the three dynamical regimes occurring in active gels. Left panel shows the configuration of the nematic field (white rods) during the relaxing dynamics in proximity of two oppositely charged semi-integer defects in the quiescent regime (*i.e.* at low activity $\zeta = 10^{-5}$). Central panel shows a configuration at $\zeta = 5 \times 10^{-4}$ in the spontaneous flow regime. The nematic field undergoes an activity-induced banding instability that breaks the rotational symmetry, producing bands of laminar flow (colored arrows) which is stronger where elastic deformations are more pronounced. Inset shows a configuration at $\zeta = 2 \times 10^{-3}$, characterized by the formation of several lanes flowing in an alternating fashion. Right panel shows a typical chaotic configuration at strong activity $\zeta = 5 \times 10^{-2}$, where rotational symmetry is statistically restored. This state is characterized by the formation of *walls*, narrow regions of strong banding deformations, which eventually give rise to the enucleation of topological defects. Simulations are performed on a square grid of size $L = 512$ and different portions of the systems are shown in the three panels.

where the label k is to intend as the wavenumber associated to the wavelength $2\pi k/L$. I remember that E_k is the energy spectrum and $\mathcal{T}_k$ is the rate at which energy is transferred by non-linear advective interactions. The terms on the right-hand side of Eq. (20) are respectively given by

$$\mathcal{S}_k^{visc} = 2\pi i \langle \mathbf{v}_\mathbf{k}^* \otimes \mathbf{k} : \sigma_\mathbf{k}^{visc} \rangle / L = -\frac{8\pi^2 \eta}{L^2} k^2 E_k$$

$$\mathcal{S}_k^{el} = 2\pi i \langle \mathbf{v}_\mathbf{k}^* \otimes \mathbf{k} : \sigma_\mathbf{k}^{el} \rangle / L$$

$$\mathcal{S}_k^{act} = 2\pi i \langle \mathbf{v}_\mathbf{k}^* \otimes \mathbf{k} : \sigma_\mathbf{k}^{act} \rangle / L$$

and represent the rate at which energy is absorbed, injected or –eventually– transferred among length-scales, by viscous, elastic and active contributions.

For the case with smallest activity at $\zeta = 5 \times 10^{-4}$ in the spontaneous flow regime, I observe that the flow develops fluctuations at the same length-scale where energy is injected, giving rise to the laminar flow observed in panel (b) of Fig. 8. As activity increases, the active stress injects energy at larger and larger wave-numbers, thus strengthening the bending of the active nematics, leading to the presence of narrow regions, *walls*, characterized by strong deformations which eventually produce a proliferation of topological defects (point-like disclinations). Walls and disclinations play a relevant role on the onset of the chaotic regime since the strong distortions in their neighborhood generate flows which are in turn responsible for the deformation of the walls and the unbinding of more defects pairs, thus driving the system towards the apparently *turbulent* state.

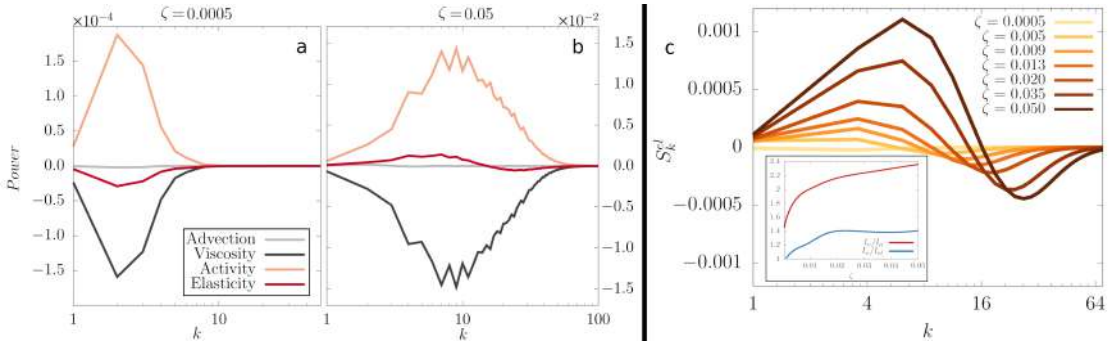

Figure 9: **Energy balance in Fourier space and elastic energy transfer.** Time averaged power spectra at $K = 0.04$, for the spontaneous flow regime at $\zeta = 5 \times 10^{-4}$ are shown in panel (a) and for the chaotic regime at $\zeta = 5 \times 10^{-2}$ in panel (b). Notice that the strength of active injection (and viscous dissipation) increases by a factor $\sim 10^2$. Panel (c) shows the elastic spectra S_k^{el} for some values of ζ and $K = 0.04$. The red (blue) line in the inset shows the ratio between the typical flow scale l_v and the active injection l_a (elastic $l_{el} = L/k_{el}$) length-scale.

In order to achieve a better understanding of the energy transfer in our system, we analyzed the energy balance in Fourier space by considering the scale-to-scale contributions of the terms in Eq. (20), shown in Fig. 9. I observe that in the spontaneous flow regime (left panel, corresponding to Fig. 8) only small wave-numbers contribute to dynamics. This is because activity is only able to excite smooth long-ranged deformations of the LC pattern which set up and autonomously maintain laminar flows spanning the whole system. The energy injected by activity (ochre line) is either dissipated by viscosity (gray) or used to sustain deformations in the LC pattern (red), leading to a localized balance, scale-by-scale, for the energy dynamics.

As ζ is increased and the system enters the chaotic regime, the rate of active injection considerably increases as activity excites modes at larger and larger wave-numbers, while the energy scale of elastic effects remains roughly unaltered, as suggested by a direct comparison of panels (a) and (b) in Fig. 9. In agreement with previous works, the dynamics is basically driven by the local balancing between active injection and viscous dissipation, while hydrodynamic convective interactions are practically negligible (grey curve) in line with the small Reynolds number measured from simulation which never exceeds 0.1.

Interestingly enough, I observe here that the elastic term change sign developing a (small) non linear energy transfer from large towards small wave-numbers (see central panel of Fig. 9), due to cross-triadic interactions in $\mathcal{S}_k^{el}$ between the nematic tensor σ^{el} and the velocity field, thus opening the road to have an equilibrium parameter in the system to control the flow response.

In this case, the behavior of the elastic contribution develops a positive branch at small wave-numbers and a negative one at large k, giving rise to an effective energy transfer from small towards larger length-scales. The amount of energy transferred among scales grows with ζ and the elastic term behaves as an energy source, since the positive branch at small wave-numbers is always larger than its negative counterpart at larger k. The elastic non-linear term moves an amount of energy which is *small*, if compared with the other contribution, over a limited range of scales so that energy is *mostly* dissipated at the same scale where it is injected. Moreover, if the elastic transfer would play a relevant role, one would expect the statistical properties of the flow to develop scale-invariant features –*i.e.* a power low decay of the energy spectrum as in hydrodynamic turbulence– in contrast with our observations.

These results suggest that the elastic term does not establish an energy cascade even con-

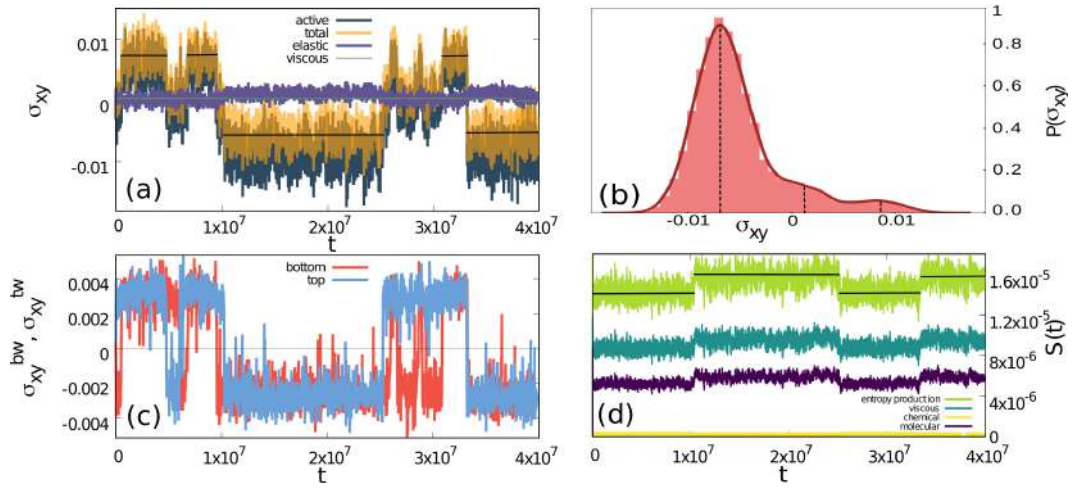

Figure 10: *Entropy production in multistable states.* (a) Time evolution of stress contributions at $Er_{act} = 1.14$,$Er = 0.00075$. The total stress is plotted in transparent yellow, while the active one is the dark blue curve underneath. Panel (b) shows the *pdf* of the total stress (data from 40 independent runs, fitted by 3 normal distributions peaked at $\sigma_{xy} = -0.0068, 0.0009, 0.0086$). (c) Total stress close to bottom and top walls, respectively computed as $\sigma_{xy}^{tw} = \int dx \int_{Ly-l}^{Ly} dy\ \sigma_{xy}$ and $\sigma_{xy}^{bw} = \int dx \int_{0}^{l} dy\ \sigma_{xy}$, where l is the width of the layer. Here $l = 15$. Nevertheless, as long as $l < Ly/2$, results remain unaltered. (d) Entropy production. Negative viscosity states, corresponding to **--** configurations of polarization at the boundaries, live longer than others. Entropy production $s(t)$ assumes greater values in correspondence of these regions.

tributing to the overall dynamics with a small non-linear transfer. This is the result –more than the cause– of the tendency of the LC to relax deformations induced by activity at small scales, giving rise to the typical configuration of Fig. 8 where narrow *walls* of strong bend deformations in the nematic pattern are spaced by wider aligned regions.

7 Rheology of Extensile Emulsions

In order to study the rheology of the active emulsion I considered a symmetric extensile emulsion (whose morphological features have already been analyzed in Section 3) under an externally imposed shear flow [6]. To do this I confined the system between two parallel moving walls with no-slip boundary conditions. The two walls move in opposite directions with velocity $\pm v_w$ so that the shear rate is given by $\dot{\gamma} = \frac{2v_w}{L}$, being L the channel width. Strong parallel anchoring was imposed for the polarization field at the wall site. In order to compare external and active forcing I consider the Ericksen number $Er = \eta_0 \dot{\gamma}/B$, and the active Ericksen number $Er_{act} = \zeta/B$, where B is the lamellar compression modulus, namely the energy cost for the variation of the lamellar width per unit length.

The most interesting behavior is found for large values of both shear rates and activity. Under this conditions the system exhibits an intermittent flow regime. This is to be related with the polarization configuration at the walls site ($\boldsymbol{P}$ can be parallel or antiparallel to the velocity on each wall, or can be parallel on a wall and antiparallel to the other and I will denote these three state with the notation $++$, $--$ and $+-$ respectively). During the evolution the system jumps between these three states. Such intermittent behavior is reflected in the evolution if the averaged stress as shown in Fig. 10. Elastic contributions are on average constant, while

active stress fluctuates around positive, negative or vanishing values that also correspond to $++$, $--$ and $+-$ states respectively. These are found to be largely determined by the portion of the system closer to boundaries. Nevertheless, not all the states are equally probable: as shown by the *pdf* of the stress tensor in panel (b), thus suggesting the $--$ states to be more likely to occur than others. In order to better characterize the physics beyond this multistable dynamics I considered the different entropy production contributions are shown due to reactive, dissipative and source effects. We first notice that the contribution due to diffusion/chemical (yellow line) is almost null. In addition, the viscous dissipation (blue line) is always greater than the contribution due to the molecular field (violet line). This suggests that the hydrodynamics of the system – driven by active injection and external forcing – is mainly countered by viscous dissipation phenomena. Moreover, the total entropy production oscillates around two different values and jumps during time evolution, with the highest value corresponding to the negative viscosity states. This behaviour is compatible with a maximum entropy production principle (MaxEPP).

Schools

- Summer school on Parallel Computing 2017 – Cineca (Bologna)
- Advanced School on Parallel Computing 2018 – Cineca (Bologna)
- XXX National Seminar of Nuclear and Subnuclear Physics "Francesco Romano" Otranto

Conference and Workshops

- SM&FT - Bari 2018;
- APS - Division of Fluid Mechanics 2018; Atlanta (USA)
- XXIII National Conference on Statistical Physics and Complex Systems; Parma
- FisMat2019 - Catania
- APS - Division of Fluid Mechanics 2019; Seattle (USA)
- Workshop INFN FieldTurb; Roma 2020
- Italian Soft Days 2020; Virtual Edition
- ESCI 2020; Virtual Edition

Offsite periods

- November 2018, Visit to prof. Biferale, Tor Vergata.
- March-April 2019 HPC Europa3 grant, Edinburgh, under the supervision of Prof. D. Marenduzzo.
- May 2019, Visit to prof. Biferale, Tor Vergata.
- July 2019, Visit to prof. Sagues, Barcelona.
- December 2019 - January 2020 HPC Europa3 grant, Edinburgh, under the supervision of Prof. D. Marenduzzo.

Teaching

- Peer Tutor 2018/2019 (Dipartimento di Fisica)
- Corso di preparazione alle materie di base (Fisica) - Poliba 2018/2019
- Peer Tutor 2019/2020 (Dipartimento di Fisica)

Publications

1 G. Negro, **L.N. Carenza**, P. Digregorio, G. Gonnella, and A. Lamura. Morphology and flow patterns in highly asymmetric active emulsions. Physica A, 503:464 – 475, 2018.

2 F. Bonelli, **L.N. Carenza**, G. Gonnella, D. Marenduzzo, E. Orlandini, and A. Tiribocchi. Lamellar ordering, droplet formation and phase inversion in exotic active emulsions. Scientific Reports, 9, 2019.

3 **L.N. Carenza**, G. Gonnella, A. Lamura, G. Negro. Dynamically asymmetric and bicontinuous morphologies in active emulsions, International Journal of Modern Physics C, 2019.

4 G. Negro, **L.N. Carenza**, P. Digregorio, G. Gonnella, A. Lamura. In silico characterization of asymmetric active polar emulsions, AIP Conference Proceedings 2071 (1), 020012, 2019.

5 **L.N. Carenza**, G. Gonnella, A. Lamura, G. Negro, A. Tiribocchi. Lattice Boltzmann methods and active fluids. Eur. Phys. J. E, 42(6):81, 2019.

6 G. Negro, **L.N. Carenza**, A. Lamura, A. Tiribocchi and G. Gonnella. Rheology of active polar emulsions: from linear to unidirectional and unviscid flow, and intermittent viscosity. Soft Matter, 15:8251–8265, 2019.

7 **L.N. Carenza**, G. Gonnella, D. Marenduzzo, G. Negro.Rotation and propulsion in 3d active chiral droplets. Proc. Natl. Acad. Sci., 116(44):22065–22070, 2019.

8 **L.N. Carenza**, G. Gonnella, L. Biferale. Multi-scale control of active emulsion dynamics. Phys. Rev. Fluids, 5:011302, 2020.

9 **L.N. Carenza**, G. Gonnella, A. Lamura, D. Marenduzzo, and G. Negro. Soft channel formation and symmetry breaking in exotic active emulsions. Sci. Rep., 10, 2020.

10 **L.N. Carenza**, G. Gonnella, D. Marenduzzo, and G. Negro. Chaotic and periodical dynamics of active chiral droplets. Physica A, 559:125025, 2020.

11 **L.N. Carenza**, G. Gonnella, and G. Negro. Lattice Boltzmann simulations of self- propelling chiral active droplets. Gangemi Editore, 2020.

12 **L.N. Carenza**, M. Giordano, G. Gonnella, and G. Negro. Activity induced isotropic-polar transition in active liquid crystals. Under Review, 2020.

13 **L.N. Carenza**, L. Biferale, and G. Gonnella. Cascade or not cascade? Energy Transfer and Elastic Effects in Active Nematics. Under Review, 2020.

14 **L.N. Carenza**, G. Gonnella, D. Marenduzzo, and G. Negro. Yielding transition occurs in multicomponent fluids. In preparation, 2020.

15 **L.N. Carenza**, G. Gonnella, D. Marenduzzo, and G. Negro. Shear yielding and percolation transition is smectics. In preparation, 2020.

16 **L.N. Carenza**, G. Gonnella, D. Marenduzzo, G. Negro, and E. Orlandini. Quasi-crystal and amorphous states of blue phases in non-euclidean geometries. In preparation, 2020.

17 **L.N. Carenza**, F. Corberi, G. Gonnella, and G. Negro. Stable negative viscosities in active emulsions. In preparation, 2020.